Oil Shale, 2026, 43, 1, 75–103 https://doi.org/10.3176/oil.2026.1.04

Genesis and depositional environment of organic-rich sediments in the Neogene organic-rich sediments from the Aleksinac deposit (Serbia): Part B

Gordana Gajica[(a)]*, Aleksandra Šajnović[(a)], Ksenija Stojanović[(b)], Milan D. Antonijević[(c)], Aleksandar Kostić[(d)], Branimir Jovančićević[(b)]

[(a)] Center of Chemistry – Institute of Chemistry, Technology and Metallurgy, University of Belgrade, Njegoševa 12, 11000 Belgrade, Serbia
[(b)] Faculty of Chemistry, University of Belgrade, Studentski trg 12-16, 11000 Belgrade, Serbia
[(c)] School of Chemistry and Chemical Engineering, University of Surrey, Guildford, Surrey GU2 7XH, United Kingdom
[(d)] Faculty of Mining and Geology, University of Belgrade, Đušina 7, 11000 Belgrade, Serbia

Received 30 April 2025, accepted 23 January 2026, available online 29 January 2026

Abstract. *To determine the characteristics of the palaeoenvironment that affected organic richness, the Neogene organic-rich sediments in the Upper layer of the Aleksinac deposit (Dubrava block, Serbia) were examined. The studied samples are presumed to be of andesitic to felsic origin, with evidence of volcanic activity. Sediment generation was influenced by hydrothermal fluids, which promoted the productivity of aquatic organisms and led to organic enrichment. Clastic input brought trace and rare earth elements into the basin. Palaeoenvironmental indicators derived from concentrations of major, trace, and rare earth elements show good accordance with organic geochemical data obtained in previous detailed studies, indicating deposition of the sediments in an anoxic lacustrine environment of variable salinity under warm, arid, and semiarid/semihumid climatic conditions. Such settings favoured primary bioproductivity in the lake, whereas a stable, stratified water column with highly reducing bottom water enhanced organic matter preservation. The lowering of total organic carbon content was mainly controlled by more humid episodes that promoted clastic influx and decreased organic matter concentration, rather than by changes in anoxic redox conditions.*

Keywords**:** *organic-rich sediments, inorganic proxies, palaeoenvironment.*

* Corresponding author, gordana.gajica@ihtm.bg.ac.rs

1. Introduction

Oil shale is mostly composed of inorganic matter, with organic matter (OM) dispersed within it, forming a homogeneous mixture. It is often characterised by fine lamination that alternates between laminae of mixed organic and mineral materials and pure mineral material. Although OM is present in a seemingly small percentage, it is very important, since it mainly contains kerogen types I and II, which have great potential to produce liquid hydrocarbons under suitable geological conditions or through thermal processing [1]. Low concentrations of trace and rare earth elements (TEs and REEs, respectively) can be found in oil shale. These elements do not exist independently and may be present as organometallic compounds, embedded in mineral crystal structures, or in a dispersed state on clay and oxyhydroxide particles [2]. Their distributions are mainly influenced by the geochemical cycle of elements and controlled by the physical and chemical characteristics of their atoms or ions, as well as by biotic and abiotic factors in the depositional environment [3, 4].

The analysis of the inorganic matter in oil shale can be used to reconstruct the geological history of the study area based on the content and distribution of elements, as well as corresponding geochemical parameters. This, in turn, allows us to determine the source material and palaeoconditions in the depositional environment that contributed to OM supply, its preservation, and the formation of organic-rich sediments, such as oil shales [1]. The main factors that control OM enrichment are palaeobioproductivity, conditions in the palaeoenvironment (climate, salinity, and redox potential), and the influx of clastic material [5–12].

Although the Aleksinac oil shale deposit is the largest and richest oil shale deposit in Serbia and of economic significance [13, 14], there are only a few studies on its inorganic composition. Therefore, the aims of this study were: (i) to establish comprehensive characteristics of the palaeoenvironment that affected the organic richness of the sediments based on inorganic proxies, and (ii) to examine the compatibility between inorganic and organic geochemical parameters. The results of this study may serve as a valuable archive of palaeoenvironmental information on the area and can be transposed to other geological scenarios.

2. Samples and analytical methods

2.1. Samples

Outcrop samples from the Upper layer of the Dubrava block of the Aleksinac deposit were selected for this study. In previous publications, a detailed description of the lithostratigraphic column of the analysed samples has been provided [15, 16], as well as in Part A of this study (see this issue).

2.2. Previous results

The origin, depositional environment, maturity and hydrocarbon generation potential of the organic matter, derived from the comprehensive OM characterisation of the analysed samples, are detailed in prior studies [15–17]. To have a better understanding of the depositional environment, these results are utilised to correlate with inorganic geochemical parameters but are not presented in this work. In this section, the main findings obtained previously are summarised, as they will be used to correlate with inorganic parameters.

The OM is uniformly immature, with total organic carbon (TOC) content varying between 1.31 and 29.10 wt% (corresponding to vitrinite reflectance of 0.36–0.44% and a production index of 0.01–0.02). Sample D16 has the highest OM content, whereas samples D4, D6, and D7 have the lowest. According to Rock-Eval data, the OM mainly consists of a mixture of kerogen types I and II. The samples that stand out are sample D13, which contains exclusively kerogen type I, and samples D4, D6, and D7, which contain kerogen type II with a certain input of kerogen type III.

The biomarker patterns are in accordance with the Rock-Eval data, revealing a significant presence of aquatic organisms, including green and brown algae, as well as bacteria, with a moderate influence from higher-plant organic matter [16, 17]. Based on the thermal decomposition of kerogen, all samples show a high potential for oil generation. Only samples D4, D6, and D7 have a slightly lower potential, which agrees with the type of kerogen in these samples [15–17].

The OM was deposited in a reducing lacustrine environment characterised by alkaline, brackish to freshwater conditions and water-column stratification, most likely as a result of variations in water depth, salinity, and temperature during the formation of the analysed sediments [16]. According to biomarker patterns in the samples under investigation, sample D16 differs most from the others [16, 17]. A shallow water column may have contributed to the relative abundance of C_{29} hopane in sample D16, whereas a steranes/hopanes ratio < 1 suggests a higher presence of prokaryotic OM than algal.

2.3. Analytical methods

For the determination of major elements, inductively coupled plasma optical emission spectroscopy (ICP-OES, Thermo iCAP 6500) was used, whereas for TEs and REEs, inductively coupled plasma mass spectrometry (ICP-MS, Thermo X Series II ICP-MS) was applied. The mineral composition was analysed using an XRD analyser (Bruker D8 Advance diffractometer). A Rock-Eval 6 Standard analyser was employed for the determination of TOC, and an elemental analyser (Vario EL III, CHNOS Elemental Analyser, Elementar Analysensysteme GmbH) for total sulphur (TS) content. Detailed analytical procedures are given in Part A of this study.

3. Results and discussion

3.1. Genesis and depositional environment of organic-rich sediments

Many geochemical parameters (Table 1) were used to determine sediment provenance, tectonic settings, the influx of hydrothermal fluids, palaeobio-productivity, clastic influx, palaeoconditions in the water column (redox potential, salinity), and climatic conditions, in order to get a better insight into the depositional environment and the genesis of organic-rich sediments of the Aleksinac deposit. The element concentrations on which the parameters were calculated are given in Part A of this study (section 3.1).

3.1.1. Sediment provenance

It is well known that the nature of the parent rocks influences the composition of sedimentary rocks [18–21]. The Al/Ti ratio and the Al vs Ti diagram are used to determine the provenance of sedimentary rocks because Al and Ti have low solubility in water. Therefore, their ratio is relatively close to that of the source rocks [20, 22–24]. Most samples have Al/Ti ratio values around 20, i.e. within the range of 8–21, which indicates intermediate igneous rock sources (Table 1) [20]. A few samples (D1, D4, D11) have values slightly higher than 21, signifying an origin from felsic igneous rocks. However, all of them are plotted near the boundary line between intermediate and felsic rocks, except for sample D16 (Al/Ti = 34; Table 1), which relates to a felsic source (Fig. 1a) [20].

The Ti vs Zr, Th/Sc vs Zr/Sc, and Co/Th vs La/Sc diagrams are also used to determine sediment provenance, since La, Th, Co, and Sc are immobile elements whose distribution is less affected by the heavy-mineral fraction than TEs such as Zr, and they are only weakly influenced by diagenesis and metamorphism [18, 24, 28]. Furthermore, La and Th are more concentrated in felsic rocks, whereas Sc and Co are more abundant in mafic rocks [26, 29]. In the Ti vs Zr diagram (Fig. 1b), all samples are located in the area of intermediate igneous rocks; only sample D16 is at the border between intermediate and felsic igneous rocks. In the Th/Sc vs Zr/Sc diagram (Fig. 1c) [18], all analysed samples are plotted in the area of felsic source rocks and have not experienced sedimentary recycling. Consistent with the results from Figure 1c, the Co/Th vs La/Sc diagram (Fig. 1d) suggests that most of the analysed samples correspond to a source between andesite and felsic volcanic rocks. According to this diagram, samples D11, D14, and D16 are more closely related to andesites and can be distinguished from the others.

A volcanic origin is not surprising, since volcanic activity in the area of the Aleksinac deposit during the Miocene has been proven, and volcanic material was transported into the lake in smaller amounts but over a longer period [30, 31]. Further evidence of volcanic activity is the presence of zeolite-group minerals – analcime and natrolite – in all samples except D16 (fig. 1 in Part A).

Table 1. Values of geochemical parameters

Parameter	D1	D2	D3	D4	D5	D6	D7	D8	D9	D10	D11	D12	D13	D14	D15	D16
Al/Ti	23.49	20.20	20.05	23.29	21.98	20.11	21.91	20.92	21.40	19.52	22.25	20.85	20.16	20.39	20.63	34.20
L/H	6.36	6.86	7.84	6.91	9.56	8.02	7.87	7.57	8.45	5.59	8.95	8.64	7.45	8.73	7.55	8.20
Ce/Ce*	0.87	0.87	0.90	0.93	0.91	0.98	0.88	0.89	0.86	0.91	0.92	0.89	0.85	0.86	0.88	0.84
Eu/Eu*	1.02	0.98	0.99	0.99	1.01	1.00	1.00	1.00	0.97	1.01	0.98	0.99	1.01	0.97	1.00	1.15
Ba/Ti	623.25	869.00	743.71	665.32	664.68	681.2	678.9	705.84	567.87	718.24	645.62	725.07	887.23	680.22	738.32	2266.07
Ba/Al	26.54	43.02	37.1	28.57	30.23	33.87	30.98	33.74	26.54	36.79	29.01	34.78	44	33.36	35.79	66.26
Ti/Al	0.04	0.05	0.05	0.04	0.05	0.05	0.05	0.05	0.05	0.05	0.04	0.05	0.05	0.05	0.05	0.03
Si/Al	2.41	3.52	2.75	2.49	3.10	2.51	2.62	2.94	2.83	2.67	2.92	2.93	3.45	2.99	2.85	3.46
∑MCE	64.86	43.63	53.62	66.45	60.20	66.72	66.71	55.14	66.04	51.73	58.95	51.78	40.79	55.67	48.58	24.10
∑TCE	152.18	102.11	140.00	185.02	120.79	204.93	180.67	156.89	134.04	142.76	111.62	131.14	100.98	118.25	127.02	55.73
∑CE	217.04	145.74	193.62	251.47	180.99	271.65	247.38	212.03	200.08	194.49	170.57	182.92	141.77	173.92	175.60	79.83
C-value	0.42	0.17	0.27	0.48	0.30	0.25	0.39	0.26	0.52	0.29	0.36	0.30	0.21	0.36	0.29	0.32
Rb/Sr	0.36	0.10	0.19	0.34	0.25	0.27	0.28	0.18	0.53	0.22	0.27	0.18	0.11	0.27	0.17	0.04
Sr/Cu	2.64	12.26	7.04	1.91	6.07	5.80	3.41	10.14	2.27	5.92	4.64	5.83	11.95	5.56	7.55	73.74
Sr/Ba	0.63	1.90	1.18	0.51	1.14	0.75	0.68	1.34	0.6	0.98	1.13	1.18	1.69	1.1	1.26	4.68
Ca/(Ca + Fe)	0.39	0.73	0.57	0.31	0.61	0.51	0.35	0.64	0.35	0.53	0.47	0.62	0.70	0.53	0.61	0.93
EF_{Mo}	42.93	3.67	8.30	14.13	9.70	5.39	14.88	3.92	8.28	4.80	20.23	6.30	17.28	9.71	9.25	1.12
EF_{U}	4.33	2.27	1.47	3.06	0.79	1.65	1.92	1.44	0.96	2.77	0.64	0.99	0.96	0.67	2.45	0.71
EF_{V}	1.66	1.04	1.54	2.30	1.37	1.24	1.94	1.43	1.99	1.53	1.58	1.42	1.10	1.85	1.51	0.58
EF_{Cu}	5.11	2.75	3.75	6.19	3.51	3.48	4.87	2.62	5.12	3.61	4.49	3.93	2.45	3.93	3.20	0.98
EF_{Ni}	1.32	0.71	1.18	0.86	1.09	0.93	1.25	1.00	1.30	1.03	1.40	1.21	0.92	1.27	1.04	9.61
EF_{Zn}	2.26	0.91	1.47	1.76	1.36	1.46	2.10	1.42	1.79	1.54	1.66	1.33	1.20	1.65	1.46	0.48
V/(V + Ni)	0.75	0.78	0.76	0.87	0.75	0.77	0.79	0.78	0.79	0.78	0.73	0.74	0.74	0.78	0.78	0.13
V/Zn	1.11	1.72	1.58	1.97	1.52	1.29	1.40	1.52	1.67	1.50	1.43	1.61	1.39	1.69	1.56	1.83

LREE/HREE = light REEs / heavy REEs; Ce anomaly, $Ce/Ce^* = Ce_N / (La_N + Pr_N)^{1/2}$ (subscript $_N$ represents PAAS-normalised values) [25]; Eu anomaly, $Eu/Eu^* = Eu_N / (Sm_N + Gd_N)^{1/2}$; ∑MCE – sum of major clastic elements = Al + Si + Ti; ∑TCE – sum of trace clastic elements = Zr + Hf + Nb + Th + Th + La + Ce; ∑CE – sum of clastic elements = ∑MCE + ∑TCE; C-value = (Fe + Mn + Cr + V + Ni + Co)/(Ca + Mg + K + Na + Sr + Ba); enrichment factors (EFs) are calculated in relation to UCC (see section 3.3 in Part A) [19, 26, 27].

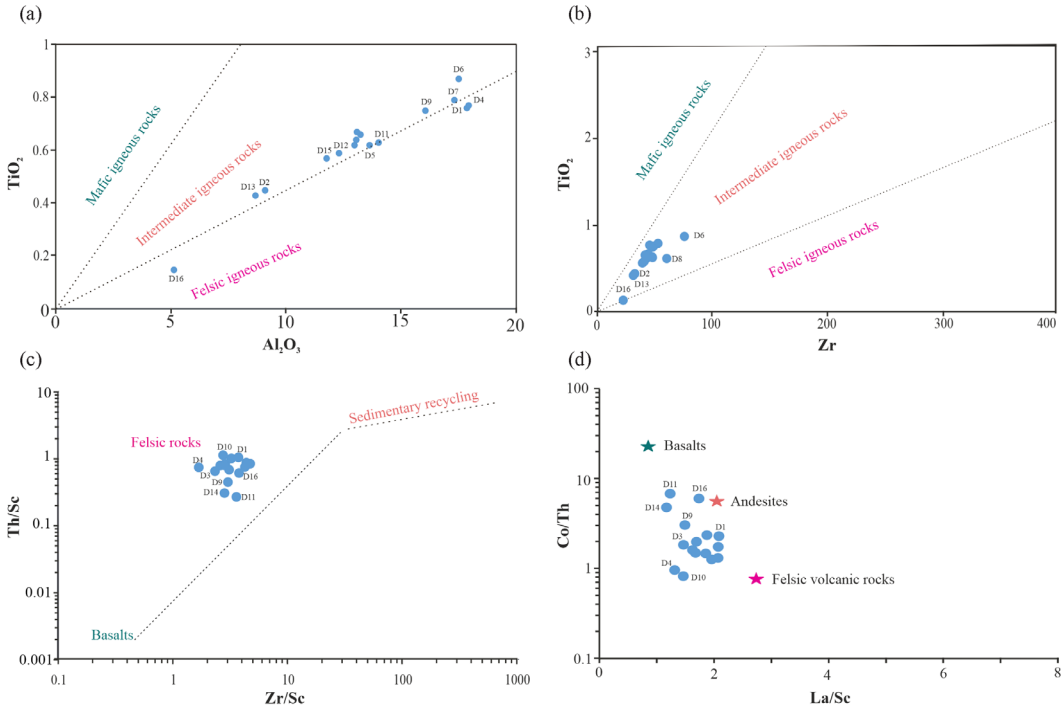

Fig. 1. Source discrimination diagrams: (a) TiO_2 vs Al_2O_3, (b) TiO_2 vs Zr, (c) Th/Sc vs Zr/Sc, and (d) Co/Th vs La/Sc.

According to Obradović and Vasić [31], analcime in the Aleksinac deposit formed through the alteration of volcanic glass, and it can also be formed by the decomposition and alteration of the earlier-phase zeolite mineral natrolite [32].

The REEs can also be used to determine sediment provenance owing to their chemical stability during different processes such as erosion, transportation, weathering, deposition, and diagenesis [18, 33, 34]. The analysed samples are characterised by high LREE/HREE ratios, which is typical of felsic rock provenance (Table 1; fig. 3 in Part A) [26, 28, 29, 35]. In oil shale, their main sources are terrigenous inherited minerals and authigenic components [36]. The statistically significant positive correlations of REEs with constituents of clastic minerals and negative correlations with carbonates (section 3.2 in Part A) indicate a terrigenous origin.

3.1.2. Tectonic settings

The plate tectonic settings of the sediment source area are important due to terrain-specific signatures and influence on the geochemical composition of deposited sedimentary rocks [23, 37–40]. Some elements are inactive during transportation and deposition, and therefore reflect different tectonic settings [39, 41].

The cross-plot K/Na vs Si (Fig. 2a) shows that most of the analysed samples were deposited in an active continental margin, while only samples D5, D6, and D9 correspond to a passive continental margin [40, 42]. Conversely, the ternary diagrams Ca–K–Na and La–Th–Sc [39] show that most of the analysed samples plot within the field of a continental island arc (Fig. 2b).

The results imply that the sediments developed in terrain with the characteristics of an active continental margin built on a continental island arc. The obtained data are not surprising, since the region of the Aleksinac deposit is known for its very complex tectonic settings, caused by the convergence of several oceanic and continental entities in the Tethyan realm between the African and European plates [43]. This resulted in the formation of four geotectonic units: the Dinarides, Carpatho-Balkanides, Serbian–Macedonian Massif, and Pannonian Basin [14, 43, 44]. According to Obradović and Vasić [31], the Aleksinac deposit was formed by the fragmentation of two geotectonic units, the Carpatho-Balkanides and the Serbian–Macedonian Massif.

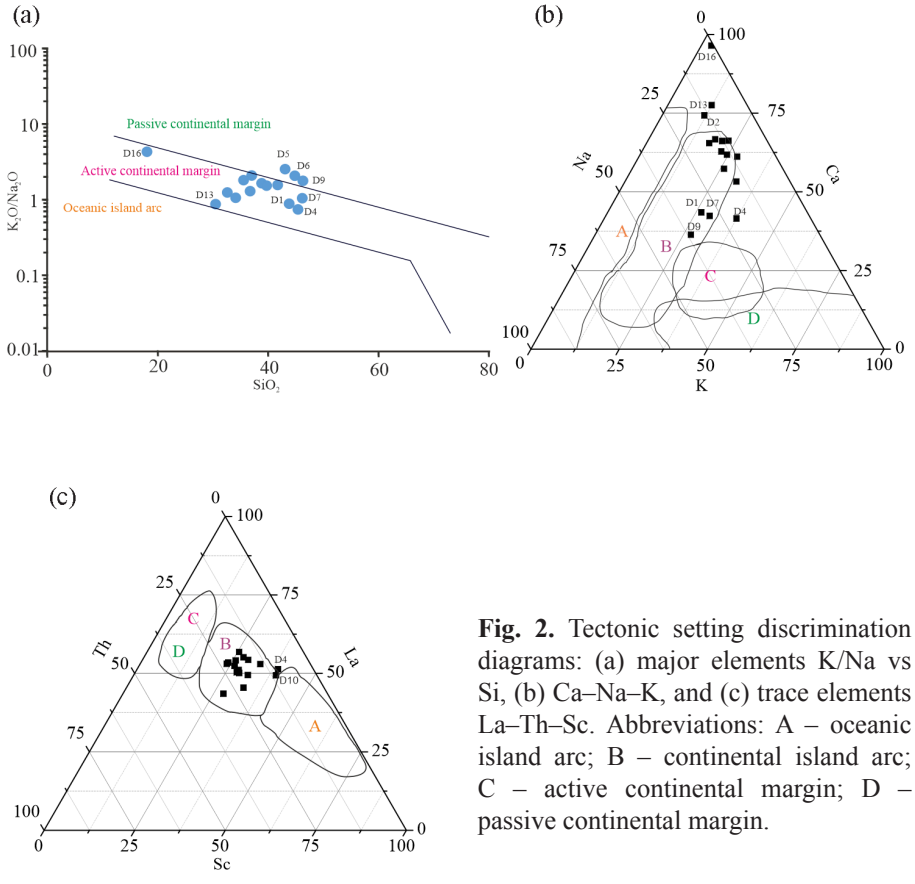

Fig. 2. Tectonic setting discrimination diagrams: (a) major elements K/Na vs Si, (b) Ca–Na–K, and (c) trace elements La–Th–Sc. Abbreviations: A – oceanic island arc; B – continental island arc; C – active continental margin; D – passive continental margin.

3.1.3. Hydrothermal fluids

Hydrothermal fluids mainly occur due to volcanic eruptions, lithification processes, and atmospheric deposition, causing the input of certain elements into deposits. They play a significant role in different geological processes. A large amount of minerals and nutrients can be transported into the lake by hydrothermal fluids, which usually promote the productivity of aquatic organisms and, consequently, may lead to OM enrichment in sediments [45, 46].

TEs (Zn, Ni, Cu) and REEs (La, Ce) can be enriched in hydrothermal fluids and, therefore, can be used to estimate whether the depositional environment was affected by hydrothermal fluids [47–49]. Furthermore, the Co/Zn vs Co + Cu + Ni (Fig. 3a) [50] and La vs Ce (Fig. 3b) [49] cross-plots, as well as the Ni–Co–Zn ternary diagram (Fig. 3c) [47, 51], were used for the estimation of hydrothermal influx.

The obtained results indicate that hydrothermal fluids influenced the analysed samples, whereas this influence was least pronounced, or absent, in sample D16 (Fig. 3). As noted previously, during the Lower Miocene there was noticeable volcanic activity (Section 3.1.1), thus the hydrothermal impact is not surprising. Additional evidence for hydrothermal fluids is provided by the presence of hydrothermal zeolite minerals, analcime and natrolite [52], identified in all samples except D16 (fig. 1 in Part A).

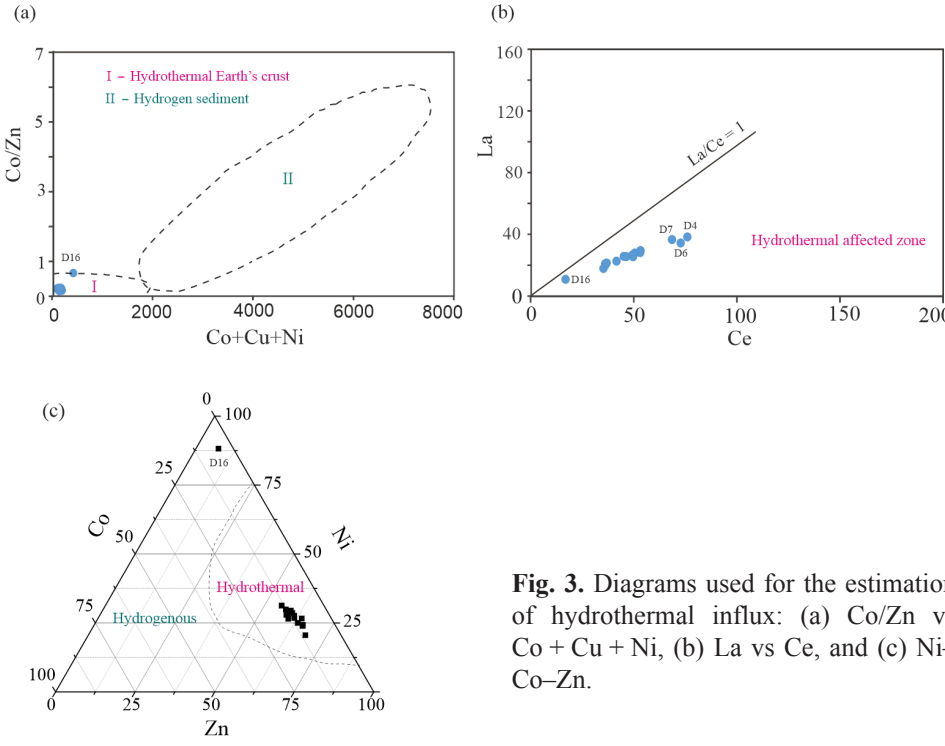

Fig. 3. Diagrams used for the estimation of hydrothermal influx: (a) Co/Zn vs Co + Cu + Ni, (b) La vs Ce, and (c) Ni–Co–Zn.

3.1.4. Palaeobioproductivity

The content of biogenic elements is associated with biological growth and can be used for the estimation of palaeobioproductivity, which is one of the main factors controlling OM content in sedimentary rocks [5, 48]. The Ba content is often used for the qualitative assessment of palaeobioproductivity, as the Ba cycle in sediments is controlled by OM content in the depositional environment [48, 53]. The Ba/Ti and Ba/Al ratios can be used to eliminate the dilution effect of OM and authigenic minerals in relation to the Ba concentration in terrigenous detrital matter [54].

The strong correlation between Ti and Al ($r = 0.97$, $p < 0.001$) in the analysed samples indicates that Al originates from terrigenous detrital matter and that biogenic processes did not affect Al concentration; thus, these ratios can be used [55]. The highest values of Ba/Ti and Ba/Al ratios are found in samples D13 and D16, which agrees with the greatest TOC content in these samples (Table 1; table 1 in Part A). Furthermore, Ba/Ti and Ba/Al ratios correlate well with TOC contents in samples D1–D15 ($r = 0.70$, $p < 0.01$; 0.68, $p < 0.01$, respectively; Fig. 4a).

The TOC content is controlled by primary bioproduction, along with redox conditions and the influx of terrigenous detrital matter into the water column. The diagram of the Cu/Mo ratio vs Cu can be used to distinguish whether the formation of organic-rich sediments resulted from increased bioproductivity or from reducing conditions [56, 57]. Specifically, high bioproductivity is usually associated with elevated Cu content, whereas Mo concentration has no impact [58]. Conversely, both Cu and Mo are enriched under anoxic conditions. Some enrichment of these elements is found in the analysed sediments (table 1 and fig. 5 in Part A). A weak statistically significant negative correlation between Cu/Mo and Cu ($r = 0.44$, $p = 0.10$; Fig. 4b) shows that, in addition to palaeobioproductivity (Fig. 4a), the enrichment of sediments in OM was also controlled by reducing conditions in the depositional environment. The same conclusion was derived from organic geochemical proxies, including the pristane/phytane ratio, gammacerane index, and abundance of β-carotane, as discussed in detail in earlier research [16].

Furthermore, the differences in TOC among D1–D15 samples can also result from varying influxes of clastic material. This is confirmed by the statistically significant positive correlation of TOC with the CaO/SiO_2 ratio ($r = 0.73$, $p < 0.01$; Fig. 4c) and will be discussed in more detail in the next section.

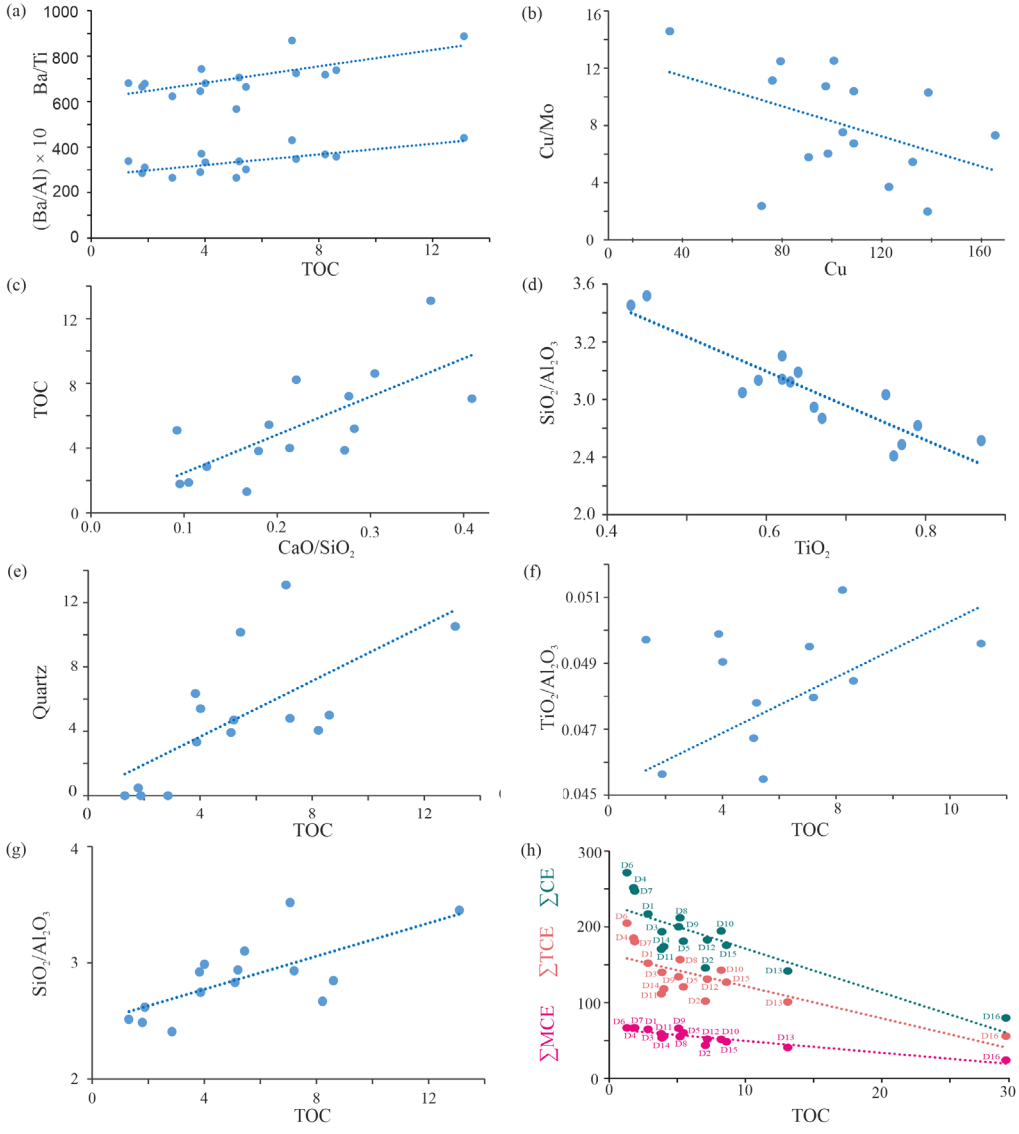

Fig. 4. Correlation diagrams between: (a) Ba/Ti and Ba/Al with TOC, (b) Cu/Mo and Cu, (c) TOC and CaO/SiO_2, (d) SiO_2/Al_2O_3 vs TiO_2, (e) quartz vs TOC, (f) TiO_2/Al_2O_3 vs TOC, g) SiO_2/Al_2O_3 vs TOC, (h) TOC and major clastic elements, trace clastic elements, and the sum of major and trace clastic elements. ∑MCE – sum of major clastic elements = (Ti + Al + Si); ∑TCE – sum of trace elements = (Zr + Th + Nb + Hf + La + Ce); ∑CE – sum of clastic elements = ∑MCE + ∑TCE.

3.1.5. Influx of clastic material

The clastic influx can induce both OM preservation (through a faster sedimentation rate, which reduces the intensity of OM degradation by aerobic microbial communities in the water column) and the dilution of OM concentration (through increased input of clastic material). In addition, clastic influx affects the type of both mineral and organic matter in the oil shale [24]. Furthermore, a greater input of clastic material increases nutrient supply, which can cause blooms of aquatic organisms and facilitate OM enrichment [9]. Concentrations of major clastic elements (MCEs; Ti, Al, and Si) and trace clastic elements (TCEs; Zr, Th, Nb, Hf, La, and Ce) are used as proxies for clastic influx [59, 60], since they are chemically stable during transportation, weathering, and diagenesis [61].

The Ti/Al ratio is used because Ti and Al mainly occur in clastic minerals of terrigenous origin, with Al representing aluminosilicate minerals and Ti occurring in clay and heavy minerals [6, 41, 62, 63]. Statistically significant positive correlations of Al with Ti, K, and Na ($r = 0.97$, $p = 2.3 \times 10^{-9}$; $r = 0.86$, $p < 0.01$; $r = 0.75$, $p < 0.01$, respectively; Fig. 1a) indicates that these elements are associated with clastic material [64], while the correlation between Ti and Al implies that the clastic influx was probably derived from a constant source (Section 3.1.4) [65, 66]. The Ti/Al ratio values in all samples are relatively uniform (0.04–0.05), with only sample D16 slightly lower (Ti/Al = 0.03; Table 1). Additionally, similar REE distributions (fig. 3 in Part A) show a consistent source during sediment formation, closely connected with terrigenous clastic rocks, implying a stable terrestrial material supply [33].

The Si/Al ratio is used as a clastic influx proxy, representing the presence of quartz in relation to clay minerals, because Si has both clastic and biogenic origins, while Al is exclusively terrigenous [62, 67]. The values of this parameter range between 2.41–3.52. Samples D1, D4, and D6 have the lowest values, whereas samples D16, D13, and D2 have the highest (Table 1). Furthermore, a statistically significant negative correlation between Ti and the Si/Al ratio ($r = 0.90$, $p < 0.01$; Fig. 4d) indicates that a certain amount of silica originates from non-detrital input [68, 69]. Moreover, a moderate positive correlation between quartz content and TOC ($r = 0.68$, $p < 0.01$; Fig. 4e) can be indicative of a partly biogenic origin of silica from siliceous organisms (e.g. SiO_2-rich plankton) [70, 71], suggesting that OM and part of the silica were deposited and buried together [69].

The obtained Ti/Al results indicate that the detrital influx was relatively constant and, therefore, could not have been a critical factor controlling variations in OM enrichment among the studied samples ($r = 0.51$, $p = 0.05$; Fig. 4f). Conversely, the Si/Al ratio values suggest certain differences among samples D1–D15 and show a stronger correlation with TOC ($r = 0.70$, $p < 0.01$; Fig. 4g). Therefore, clastic influx could have been a significant factor influencing the formation of these organic-rich sediments. This is more evident when concentrations of clastic mineral constituents are used as proxies

for clastic influx (Fig. 4h). In Figure 4h, the strong negative correlations of TOC with MCEs and TCEs ($r \sum MCE = 0.86$, $p < 0.01$; $r \sum TCE = 0.70$, $p < 0.01$; $r \sum CE = 0.77$, $p < 0.01$) clearly indicate that clastic influx resulted in a decrease of OM concentration in the studied samples. Furthermore, the trend of samples in Figure 4 corresponds well with TOC values (table 1 in Part A).

3.1.6. Conditions in the palaeoenvironment

Climate, salinity, and redox potential are the main palaeoenvironmental proxies that control OM accumulation and preservation. The palaeoclimate is determined based on the C-value, and the Sr/Cu and Rb/Sr ratios; palaeosalinity is indicated by the Sr/Ba and Ca/(Ca + Fe) ratios, and REE distribution, while palaeoredox conditions are assessed by the EFs of Mo, U, V, Cu, and Ni, the V/(V + Ni) and V/Zn ratios, as well as by the Eu anomaly.

3.1.6.1. Climate

Most processes in the lacustrine depositional environment are controlled by climate, as it affects OM productivity, the influx of terrigenous material, and OM preservation during sediment formation [72, 73]. Consequently, according to some authors, climate can be a significant factor in the formation of OM-rich sediments (e.g. [6]).

The C-value is used to determine climate, since Fe, Mn, Cr, V, Ni, and Co are enriched in sedimentary rocks under humid climatic conditions, while Ca, Mg, K, Na, Sr, and Ba are representative of an arid climate [74, 75]. Most of the analysed samples have C-values between 0.21–0.39, suggesting semiarid conditions; the C-values for samples D1, D4, and D9 are in the range of 0.42–0.52, indicating semiarid–humid conditions, while the value for sample D2 (0.17) implies an arid climate (Table 1) [74, 75].

The Rb/Sr ratio is used to estimate palaeoclimate, since Rb precipitates and is adsorbed by clay minerals under humid conditions, whereas Sr is deposited with carbonates during dry periods [37, 76, 77]. Consequently, high values of the ratio indicate humid conditions, while low values reflect arid conditions. The majority of the samples have Rb/Sr ratios < 0.3, indicating semiarid conditions, whereas samples D1, D4, and D9 exhibit somewhat elevated values (0.34–0.53), reflecting semiarid–humid conditions, which is in accordance with the above-discussed C-value (Table 1).

The Sr/Cu ratio is based on the observation that the concentration of Sr increases under arid conditions, while the concentration of Cu rises under humid conditions. Accordingly, an elevated Sr/Cu ratio indicates a dry and warm climate [24, 78]. Most samples (D3, D5, D6, D10, D12, D14, D15) have Sr/Cu ratio values between 5–10, suggesting warm semiarid to semihumid conditions. Samples D1, D4, D7, D9, and D11 are characterised by a Sr/Cu ratio < 5, which indicates a warm and humid climate. However, in accordance with the above-discussed C-value and the Rb/Sr ratio, samples D1, D4, and D9 show the lowest Sr/Cu ratio values < 2.6, reflecting the highest

palaeoenvironmental humidity within the studied sample set. On the other hand, samples D2, D8, D13, and D16 exhibit Sr/Cu ratio values > 10, indicating dry and hot conditions [41, 75, 79]. It should be noted that sample D16, which clearly differs from the rest, also displays the most significant difference in palaeoclimate proxy values (Rb/Sr = 0.04; Sr/Cu = 73.74; Table 1), implying the most pronounced aridity within the studied set.

The climate indices C-value, Rb/Sr, and Sr/Cu show significant correlations ($r = 0.91$, $p < 0.01$; $r = –0.89$, $p < 0.01$; $r = –0.85$, $p < 0.01$, respectively). Conversely, moderate correlations of these parameters with TOC contents in samples D1–D15 ($r = –0.51$, $p = 0.05$; $r = –0.55$, $p < 0.05$; $r = 0.67$, $p < 0.01$, respectively) are observed. This may imply that increased humidity caused a higher clastic influx, which contributed more to the decrease of OM concentration than to the increase in palaeobioproductivity (i.e. blooms of aquatic organisms). It is also documented by highly similar correlation coefficients ($r = 0.5–0.7$) between the climate proxies and TOC, as well as the S2/S3 ratio (derived from Rock-Eval data discussed in [16]), reflecting the relative input of aquatic vs terrestrial OM and thus the quality of OM to produce hydrocarbons.

3.1.6.2 Salinity

Salinity in the water column is one of the key factors that control the growth of organisms in lacustrine environments and the preservation of OM [80, 81].

The Sr/Ba ratio is commonly used to estimate palaeosalinity because Sr and Ba are sensitive to salinity variations and have different geochemical behaviour [6, 82, 83]. Sr is deposited directly from seawater, while Ba is easily adsorbed by clay minerals and fine clastic sediments [84, 85]. A high Sr concentration can be an indication of the inflow of seawater into the lake; therefore, the Sr/Ba ratio increases as water salinity rises. Most of the analysed samples have Sr/Ba > 1, which implies saline water, whereas samples D1, D4, D6, D7, and D9 have values < 1, which suggests fresh water [86, 87].

The Ca/(Ca + Fe) ratio also shows sensitivity to salinity changes [88]. Most samples have Ca/(Ca + Fe) ratio values ranging from 0.47 to 0.73, indicating brackish water. The exceptions are samples D1, D4, D7, and D9, which have values of this parameter < 0.40, suggesting a freshwater environment, and sample D16, which shows a value of 0.93, indicating saline water (Table 1) [72, 88]. This is in line with conclusions derived from biomarker proxies of the analysed samples (pristane/phytane ratio, gammacerane index, and the abundance of β-carotane), which indicate deposition of OM in a lacustrine alkaline brackish to freshwater environment under warm climatic conditions [16].

A good agreement between OM richness and salinity is observed (TOC vs Sr/Ba ratio: $r = 0.70$, $p < 0.01$; TOC vs Ca/(Ca + Fe) ratio: $r = 0.60$, $p < 0.05$, for samples D1–D15). Samples D2, D13, and D16, containing the highest TOC contents, exhibit the greatest values of both palaeosalinity proxies, whereas samples D1, D4, D6, and D7, with the lowest TOC contents (< 3%), were

deposited under freshwater conditions (Table 1; table 1 in Part A). The most organic-rich sample, D16, again displays a notable difference from D1–D15, being characterised by evidently higher Sr/Ba and Ca/(Ca + Fe) ratios (4.68 and 0.93, respectively; Table 1), clearly indicating the influence of marine water. This observation is consistent with results from previous research, which also showed that during the deposition of sediments represented by D16, there was a marine inflow from the Paratethys Sea as a result of regional tilting of the area during the Lower Miocene [16].

Generally, salinity is controlled by climate, because the salinity of water increases under warm and arid conditions as a result of evaporation [89, 90]. This is also reflected within the studied sample set, since statistically significant correlations between the climate indices (C-value, Rb/Sr, Sr/Cu) and salinity proxies (Sr/Ba and Ca/(Ca + Fe)) are observed (r ranging from 0.84 to 0.94).

3.1.6.3 Redox conditions

According to some authors, anoxic conditions are the main factor regulating OM enrichment and fixation within sediments [80, 91]. Such settings are controlled by climatic and hydrographic conditions and can develop within stratified water columns due to salinity and/or temperature gradients [56]. TEs such as Cr, Ni, V, U, Th, Mo, Cu, and Co can be used as redox tracers because their oxidation state and solubility are influenced by the redox status of the palaeoenvironment [22, 56, 58, 92–94].

The analysed samples showed enrichment in Mo, U, V, Cu, Ni, and Zn (section 3.3 in Part A). The enrichment of these elements is typical of deposits formed under anoxic conditions and usually indicates that such conditions were associated with high palaeobioproductivity [7, 95]. The parameters V/(V + Ni) and V/Zn (Table 1) also indicate anoxic conditions in the depositional environment [62, 96, 97]. This agrees with conclusions drawn from biomarker proxies presented in previous studies [16, 17], which are also considered reliable indicators of redox conditions.

For more detailed monitoring, EFs for redox tracers [8, 56, 98] were calculated for each sample individually (Table 1). Interestingly, in most cases, the highest enrichment of these elements is found in samples D1, D4, and D7, which exhibit the lowest TOC contents (Table 1; table 1 in Part A). In contrast, the lowest EF values are observed for the most organic-rich sample, D16. Therefore, the obtained data may indicate that the lower TOC contents in samples D1, D4, and D7 were not caused by a change in anoxic redox conditions but rather by the dilution of OM concentration due to clastic influx (Section 3.1.5).

This interpretation is in accordance with biomarker redox proxies, which clearly indicate a stable water column level (i.e. anoxic settings) during the formation of samples D1–D15, as well as elevated values of the gammacerane index, associated with a steadily low pristane/phytane ratio, particularly in samples D1, D4, and D7 [16]. On the other hand, the lowest redox tracer EFs

for sample D16 coincide with biomarker parameters implying a shallower but stratified and more saline calm water column [16], as well as with palaeoclimate indices indicating arid and warm climatic conditions (Section 3.1.6.1).

3.2. Integrative implications for the formation of organic-rich sediments in the Dubrava block

The characteristics of the lacustrine depositional environment affect the formation of organic-rich sediments and kerogen type, and therefore their potential to produce liquid hydrocarbons. These characteristics are recorded in the geochemical features of sediments and can be obtained from analyses of both organic and inorganic matter ([5, 60, 65, 99, 100] and references therein).

Both inorganic and organic data clearly show a notable difference in sample D16 (Fig. 5a) and certain differences among samples D1–D15 (Fig. 5b). Although D16 is the only sample of its type in the analysed series, it clearly reflects the transition from a swamp environment to a lacustrine one, as well as the geological evolution of the basin.

Sample D16 was formed just above the main coal seam, which indicates significant changes in sedimentary conditions. The main factors that induced this were probably tectonic activity and climate change, which have led to a transgression [31]. Sample D16 is characterised by the highest proportion of carbonate minerals (63.87 wt%; fig. 1 in Part A), the exclusive presence of the carbonate mineral aragonite and the sulphate mineral bassanite [16], and the absence of feldspar and zeolite group minerals (natrolite and analcime). It also shows lower concentrations of almost all TEs and REEs.

Geochemical data indicate differences in provenance and tectonic settings between sample D16 (more felsic) and samples D1–D15 (Sections 3.1.1 and 3.1.2), while D16 was not influenced by hydrothermal fluids (Section 3.1.3). Sample D16 is also characterised by higher palaeobioproductivity (the highest Ba/Al and Ba/Ti ratios; Section 3.1.4) and significantly lower detrital input (the highest Si/Al ratio and the lowest concentrations of constituents of clastic minerals and TEs; Section 3.1.5; sections 3.1.1 and 3.1.3 in Part A).

The salinity parameters (Sr/Ba, Ca/(Ca + Fe); Section 3.1.6.2) indicate marine water inflow into the lake. As mentioned, sample D16 has the highest content of carbonate minerals (fig. 1 in Part A), which are associated with an arid climate and alkaline environment [101]. Moreover, the enrichment in carbonate minerals also means that there was no substantial detrital or terrestrial material influx into the lake, which led not only to OM enrichment but also to the dilution of almost all TE and REE concentrations, except for Cs, Sr, Cr, and Ni [23]. The Sr enrichment is attributed to marine transgression and the formation of a large amount of the carbonate mineral aragonite [16].

Cr and Ni are redox-sensitive elements; hence, reducing conditions favoured their enrichment in sediments [57]. The high concentration of Ni can

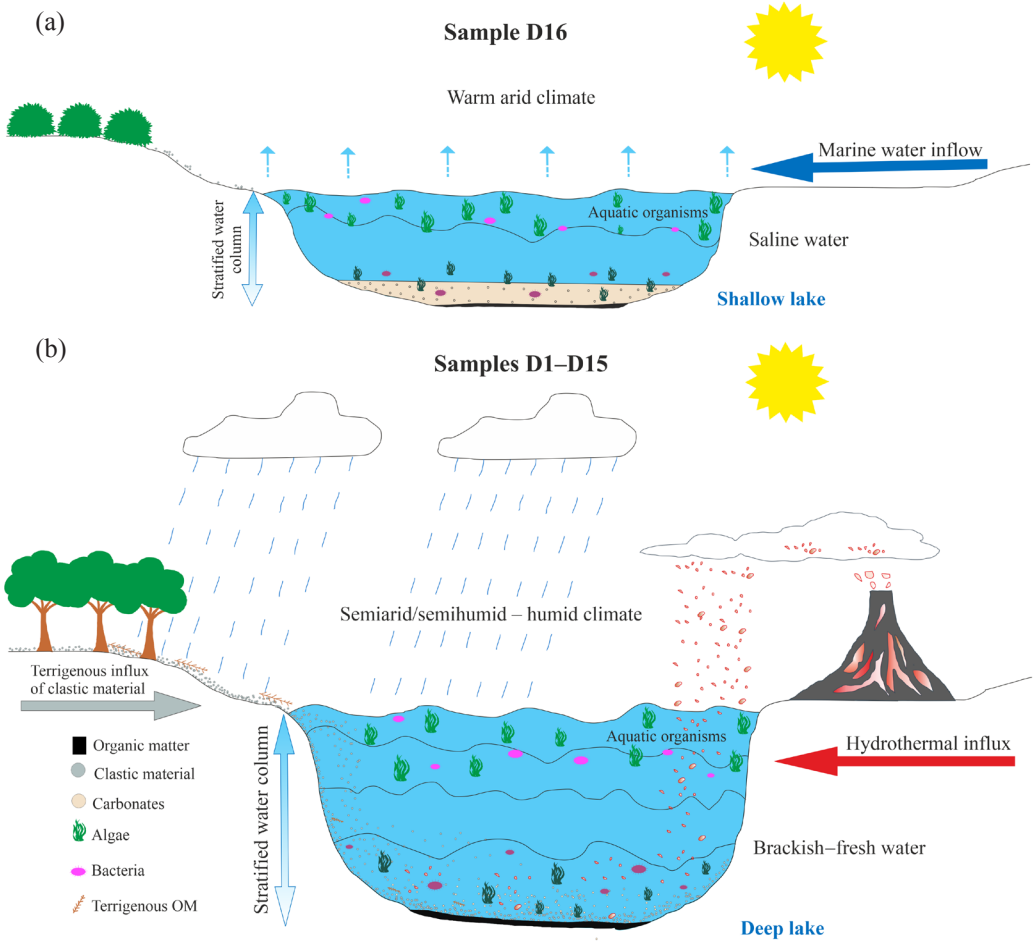

Fig. 5. Sketch illustrating the depositional environments during oil shale formation of (a) sample 16 and (b) samples D1–D15.

also originate from seawater inflow [102] and/or high OM flux [56], while a notably increased content of S can explain the enrichment of Cs in this sample only (6.11 wt%; table 1 in Part A) [103] and/or elevated water temperature [104].

During the formation of sediments represented by sample D16, the climate was warm and arid (Section 3.1.6.1; see also the presence of bassanite and aragonite in section 3.1.1 in Part A). Such conditions enhanced water evaporation, resulting in a lower water level, higher insolation, and weaker circulation within the water body, consequently favouring stratification. These conditions led to an anoxic environment at depth, which contributed to better OM preservation. Combined with high palaeobioproductivity (mainly

favourable for the growth of algae and sulphur-reducing bacteria) and a low clastic input (minimising the dilution effect on OM concentration), this resulted in the highest TOC content.

All the above observations derived from the study of inorganic components are in accordance with the detailed characterisation of OM [16, 17]. The OM study also implied a calm alkaline environment and pointed out sudden ingressions of marine water into the basin. The water column was shallow but stratified due to the somewhat increased salinity and elevated temperature. Such conditions led to high palaeobioproductivity, significant deposition, and preservation of aquatic OM (mainly algae and bacterial remnants) [16, 17].

Additionally, it is well known (e.g. [105–107]) that the sudden mixing of a thermally stratified freshwater column, caused by sporadic storms or marine water ingressions, induces oxygen deprivation and/or salt stress. Such events cause environmental shock and mass mortality of aquatic biota due to their inability to adapt, thus promoting enhanced OM deposition at the sediment–water interface and the local formation of organic-rich layers. Consequently, any of the phenomena explained above can lead to the formation of sediments extremely rich in OM (TOC 29.10 wt%; table 1 in Part A), consisting of a mixture of oil-prone kerogen types I and II [16, 17].

After the deposition of sediments represented by sample D16, the lake deepened over time, probably due to further tectonic activity (Section 3.1.2) and climate change (still warm, but more humid climate; Section 3.1.6.1). Due to the semiarid/semihumid to humid climate, freshwater inflow into the lake occurred, leading to a rise in water level (brackish–fresh lake) that is usually accompanied by a higher terrigenous influx of clastic material. The clastic influx carried nutrients into the lake, causing blooms of aquatic organisms (mainly primary producers, such as green and brown algae, and bacteria) and increasing the sedimentation rate. Generally, a faster sedimentation rate contributes to better OM preservation but also leads to its reduced concentration due to dilution by clastic material [108]. Furthermore, the freshwater inflow into the lake resulted in a very low S content in samples D1–D15 (0.06–0.23 wt%; table 1 in Part A), compared with D16 (6.11 wt%).

As the lake is a dynamic system, during the formation of sedimentary rocks represented by samples D1–D15, there were fluctuations in bioproductivity, water column level, and stratification, which were consequence of changes in humidity, freshwater inflow, and hydrothermal and clastic influx. All these factors resulted in geochemical variations among samples D1–D15, grouping them into two subclusters. One subcluster (Ib) comprises samples D1, D4, D6, D7, and D9, whereas the second (Ia) includes the remaining samples, among which a slight distinction between samples D2 and D13 is observed, with more pronounced clustering of D13 (section 3.1.3 in Part A).

The samples of subcluster Ib are characterised by the lowest TOC contents (table 1 in Part A), a high content of clay minerals, a relatively high content of feldspar minerals, absence or very low content of quartz, the lowest

amount of carbonate minerals (section 3.1.1 in Part A), high concentrations of REEs (section 3.1.4 in Part A), the highest humidity / the lowest salinity (Sections 3.1.6.1 and 3.1.6.2), and high clastic input (Section 3.1.5). This particularly applies to samples D4, D6, and D7, which show the highest influx of clastic terrigenous material, as indicated by the REE distributions (Section 3.1.1), kerogen type, and biomarkers [16]. The V/(V + Ni) and V/Zn ratios, EFs for redox tracers, and biomarker proxies (gammacerane index and pristane/phytane ratio; [16]) clearly imply anoxic redox conditions. Therefore, the lowering of TOC content in the samples of subcluster Ib can mostly be attributed to a decrease of OM concentration due to clastic influx (Section 3.1.5), rather than to a change in anoxic redox conditions. Furthermore, this also signifies that the reduced OM potential for liquid hydrocarbon generation in samples D4, D6, and D7 (i.e. the presence of type III kerogen; [16]) was mainly controlled by the clastic influx that resulted in an increased impact of allochthonous higher-plant biomass.

The samples from subcluster Ia are characterised by a substantial content of OM (with high hydrocarbon generation potential, i.e. kerogen types I and II), resulting from high palaeobioproductivity, further supported by hydrothermal fluids (as documented by the presence of analcime and natrolite and corresponding parameters; Section 3.1.3) and anoxic redox conditions (Section 3.1.6.3). A moderate clastic influx is observed. Both inorganic data and biomarker proxies suggest a relatively high and stable brackish water column, the stratification of which was supported by a warm semiarid/ semihumid climate.

Sample D13 differs from the other samples of subcluster Ia by a relatively higher TOC content (~13 wt%; table 1 in Part A), a higher content of carbonate minerals and quartz, a lower amount of feldspar and clay minerals, lower REE content, and a lower clastic input (Section 3.1.5; sections 3.1.1–3.1.3 in Part A). Among numerous parameters, the most evident distinguishing feature of sample D13 is its more pronounced aridity (Sections 3.1.6.1 and 3.1.6.2), which may have caused a lower clastic influx (similar to the case of sample D16), resulting in less OM dilution and a slight increase in alkalinity/ salinity. This calm, alkaline, arid environment was favourable for the deposition of carbonates, but also for the blooming of aquatic biota (increased nutrient concentration due to evaporation), as documented by the highest palaeobioproductivity index values (Section 3.1.4). Furthermore, the calm environment and warm conditions promoted water stratification and anoxic settings, contributing to good algal OM preservation. The obtained results are in accordance with OM proxies, which indicate the highest hydrocarbon generation potential and enrichment in precursor algal biomass in sample D13 (type I kerogen; [15–17]).

Finally, the slight separation of sample D2 (fig. 2 in Part A) can also be attributed to enhanced aridity and palaeobioproductivity. This sample showed almost equal values of ∑REEs (section 3.1.4 in Part A) and climate and

salinity proxies as sample D13 (Sections 3.1.6.1 and 3.1.6.2). In addition, it is associated with the highest carbonate content (section 3.1.1 in Part A) and palaeobioproductivity parameters (Section 3.1.4), as well as the lowest content of MCEs and TCEs after sample D13 (Section 3.1.5), among the samples comprising subcluster Ia.

It should be noted that the classification of samples based on mineral composition and concentrations of major, trace, and rare earth elements, in addition to full accordance with Rock-Eval data and biomarker proxies, and a clear indication of the main factors causing differences in organic richness, also revealed thorough consistency with lithology (Table 1; fig. 2 in Part A).

4. Conclusions

A detailed inorganic geochemical characterisation of the Upper layer of Aleksinac oil shale in the Dubrava block was performed.

An andesite to felsic origin is presumed for the studied samples, with evident volcanic activity, also documented by the presence of zeolite group minerals (analcime and natrolite). Accordingly, sediment formation was influenced by hydrothermal fluids, which promoted the productivity of aquatic organisms and thus led to OM enrichment. The sediments developed in terrain with active continental margin characteristics and were built on a continental island arc, consistent with the complex tectonic settings of the Aleksinac deposit and its formation through fragmentation of two geotectonic units, the Carpatho-Balkanides and the Serbian–Macedonian Massif.

Palaeoenvironmental indicators derived from concentrations of major, trace, and rare earth elements showed good accordance with organic geochemical data from previous detailed studies, indicating deposition of the sediments in an anoxic lacustrine environment of variable salinity (from saline to freshwater) under warm, arid, and semiarid/semihumid climatic conditions. Such conditions favoured primary bioproductivity in the lake, whereas a stably stratified water column, with highly reducing bottom water, enhanced OM preservation.

Classification of the samples based on mineral composition and concentrations of major, trace, and rare earth elements resulted in two main clusters (I and II), showing a distinct separation of two subclusters within the first group. This classification revealed good accordance with Rock-Eval data, biomarker proxies, and lithology, clearly indicating the main factors that caused differences in organic richness.

Samples D1–D15, forming the first cluster, are characterised by variable contents of clays, feldspars, quartz, carbonates, TOC (~1–13 wt%), and S (0.06 0.23 wt%), as well as concentrations of trace and rare earth elements. Within this group, samples D1, D4, D6, D7, and D9, comprising subcluster Ib, clearly stand out from the remaining samples (subcluster Ia), based on the

increased contents of all clastic constituents and rare earth elements, absence or very low content of quartz, the lowest amount of carbonate minerals, and the lowest TOC contents (~1–3 wt%).

The second cluster comprises sample D16, which notably differs from all other samples (D1–D15) and is the first sample deposited after the main coal seam. It is characterised by the highest content of carbonate minerals (63.87 wt%), OM (TOC 29.10 wt%), and S (6.11 wt%), the exclusive presence of the carbonate mineral aragonite and the sulphate mineral bassanite, the absence of feldspar and zeolite group minerals, and lower concentrations of almost all trace and rare earth elements (except Cs, Sr, Cr, and Ni). The greatest OM-enrichment in sample D16 resulted mainly from the warm and arid climate, and marine water ingressions, which created favourable conditions for primary producers, whereas the calm, alkaline, stratified anoxic water column contributed to excellent preservation of aquatic OM. Warm and arid conditions also minimised clastic input.

The main change in the depositional environment of the sediments represented by samples D1–D15 in relation to sample D16 occurred due to tectonic activity and climate change. A more humid (semiarid/semihumid, but still warm) climate, together with freshwater inflow into the lake, raised the water level (brackish–fresh lake, low S content), while maintaining the anoxic settings that promoted OM preservation, but also increasing the influx of clastic terrigenous material. Detailed analysis of palaeoenvironmental proxies, which showed accordance with biomarker parameters, clearly revealed that the lowering of TOC and the segregation of samples D1, D4, D6, D7, and D9 into a separate subcluster resulted from humid episodes that promoted clastic influx, rather than from changes in anoxic redox conditions. Furthermore, the lowering of OM potential for liquid hydrocarbon generation in samples D4, D6, and D7 (i.e. the presence of type III kerogen) was also mainly controlled by the clastic influx that resulted in the increased impact of allochthonous higher-plant biomass.

The obtained results represent valuable palaeoenvironmental records for the study area and can contribute to future exploration and utilisation of oil shale in the Aleksinac deposit.

Data availability statement

The data supporting the findings of this study are available within the article.

Acknowledgements

The study was financed by the Ministry of Education, Science and Technological Development of the Republic of Serbia (contract No. 451-03-136/2025-03/200168, project No. 451-03-136/2025-03/200026). We dedicate this paper to the memory of our colleague Prof. Dr Aleksandar Kostić, who passed away during the preparation of this manuscript. The publication costs of this article were partially covered by the Estonian Academy of Sciences.

References

1. Tissot, B. P., Welte, D. H. *Petroleum Formation and Occurrence*. 2nd ed. Springer-Verlag, Heidelberg, 1984.
2. Han, Y. W, Ma, Z. D., Zhang, H. F., Zhang, B. R., Li, F. L., Gao, S. et al. *Geochemistry*. Geological Publishing House, Beijing, 2003.
3. Aliyev, S. A., Sari, A. Organic material and trace elements of bituminous rocks in the Ozanköy Field, Ankara, Turkey. *Acta Geologica Sinica (English Edition)*, 2007, **81**(4), 658–667. https://doi.org/10.1111/j.1755–6724.2007.tb00989.x
4. Balaram, V. Rare earth elements: a review of applications, occurrence, exploration, analysis, recycling, and environmental impact. *Geoscience Frontiers*, 2019, **10**(4), 1285–1303. https://doi.org/10.1016/j.gsf.2018.12.005
5. Pedersen, T. F., Calvert, S. E. Anoxia vs. productivity: what controls the formation of organic-carbon-rich sediments and sedimentary rocks? *AAPG Bulletin*, 1990, **74**(4), 454–466. https://doi.org/10.1306/0C9B232B-1710-11D7-8645000102C1865D
6. Jia, J., Bechtel, A., Liu, Z., Strobl, S. A. I., Sun, P., Sachsenhofer, R. F. Oil shale formation in the Upper Cretaceous Nenjiang Formation of the Songliao Basin (NE China): implications from organic and inorganic geochemical analyses. *International Journal* of *Coal Geology*, 2013, **113**, 11–26. https://doi.org/10.1016/j.coal.2013.03.004
7. Song, Y., Liu, Z., Meng, Q., Xu, J., Sun, P., Cheng, L. et al. Multiple controlling factors of the enrichment of organic matter in the Upper Cretaceous oil shale sequences of the Songliao Basin, NE China: implications from geochemical analyses. *Oil Shale*, 2016, **33**(2), 142–166. https://doi.org/10.3176/oil.2016.2.04
8. Xu, S.-C., Hu, H.-B., Zhang, P., Wang, Q.-C., Kang, J., Miao, Q. Major and trace elements in mid-Eocene lacustrine oil shales of the Fushun Basin, NE China: concentration features and paleolimnological implications. *Marine and Petroleum Geology*, 2020, **121**, 104610. https://doi.org/10.1016/j.marpetgeo.2020.104610
9. Li, T.-J., Huang, Z.-L., Chen, X., Li, X.-N., Liu, J.-T. Paleoenvironment and organic matter enrichment of the Carboniferous volcanic-related source rocks in the Malang Sag, Santanghu Basin, NW China. *Petroleum Science*, 2021, **18**, 29–53. https://doi.org/10.1007/s12182-020-00514-1
10. Wu, Z., Zhao, X., Li, J., Pu, X., Tao, X., Shi, Z. et al. Paleoenvironmental modes and organic matter enrichment mechanisms of lacustrine shale in the Paleogene Shahejie Formation, Qikou Sag, Bohai Bay Basin. *Energy Reports*, 2021, **7**, 9046–9068. https://doi.org/10.1016/j.egyr.2021.11.228
11. Mallick, M., Banerjee, B., Hassan, T., Kumar, T. V., Babu, E. V. S. S. K., Krishna, K. et al. Geochemistry of Permian carbonaceous shales from Raniganj sub-basin, Damodar Valley, India: implications for provenance, weathering, tectonics and source of organic matter. *Applied Geochemistry*, 2022, **146**, 105469. https://doi.org/10.1016/j.apgeochem.2022.105469
12. Armstrong-Altrin, J. S., Ramos-Vázquez, M. A., Madhavaraju, J., Marca-

Castillo, M. E., Machain-Castillo, M. L, Márquez-García, A. Z. Geochemistry of marine sediments adjacent to the Los Tuxtlas volcanic complex, Gulf of Mexico: constraints on weathering and provenance. *Applied Geochemistry*, 2022, **141**, 105321. https://doi.org/10.1016/j.apgeochem.2022.105321

13. Ercegovac, M., Grgurović, D., Bajc, S., Vitorović, D. Oil shale in Serbia: geological and chemical-technological investigations, actual problems of exploration and feasibility studies. In *Mineral Material Complex of Serbia and Montenegro at the Crossings of Two Millenniums* (Vujić, S., ed.). Margo-Art, Belgrade, 2003, 368–378.
14. Jelenković, R., Kostić, A., Životić, D., Ercegovac, M. Mineral resources of Serbia. *Geologica Carpathica*, 2008, **59**(4), 345–361.
15. Gajica, G., Šajnović, A., Stojanović, K., Antonijević, M., Aleksić, N., Jovančićević, B. The influence of pyrolysis type on shale oil generation and its composition (Upper layer of Aleksinac oil shale, Serbia). *Journal of the Serbian Chemical Society*, 2017, **82**(12), 1461–1477. https://doi.org/10.2298/JSC170421064G
16. Gajica, G., Šajnović, A., Stojanović, K., Kostić, A., Slipper, I., Antonijević, M. et al. Organic geochemical study of the upper layer of Aleksinac oil shale in the Dubrava block, Serbia. *Oil Shale*, 2017, **34**(3), 197–218. https://doi.org/10.3176/oil.2017.3.01
17. Gajica, G., Šajnović, A., Stojanović, K., Schwarzbauer, J., Kostić, A., Jovančićević, B. A comparative study of the molecular and isotopic composition of biomarkers in immature oil shale (Aleksinac deposit, Serbia) and its liquid pyrolysis products (open and closed systems*). Marine and Petroleum Geology*, 2022, **136**, 105383. https://doi.org/10.1016/j.marpetgeo.2021.105383
18. McLennan, S. M., Hemming, S., McDaniel, D. K., Hanson, G. N. Geochemical approaches to sedimentation, provenance, and tectonics. In *Processes Controlling the Composition of Clastic Sediments* (Johnsson, M. J., Basu, A., eds). Geological Society of America, 1993, 21–40. https://doi.org/10.1130/SPE284-p21
19. Taylor, S. R., McLennan, S. M. The geochemical evolution of the continental crust. *Reviews of Geophysics*, 1995, **33**(2), 241–265. https://doi.org/10.1029/95RG00262
20. Hayashi, K.-I., Fujisawa, H., Holland, H. D., Ohmoto, H. Geochemistry of ~1.9 Ga sedimentary rocks from northeastern Labrador, Canada. *Geochimica et Cosmochimica Acta*, 1997, **61**(19), 4115–4137. https://doi.org/10.1016/S0016-7037(97)00214-7
21. Basu, A. Evolution of siliciclastic provenance inquiries: a critical appraisal. In *Sediment Provenance: Influences on Compositional Change from Source to Link* (Mazumder, R., ed.). Elsevier, Amsterdam, 2017, 5–23.
22. Fu, X., Wang, J., Feng, X., Chen, W., Wang, D., Song, C. et al. Mineralogical composition of and trace-element accumulation in lower Toarcian anoxic sediments: a case study from the Bilong Co. oil shale, eastern Tethys. *Geological Magazine*, 2016a, **153**(4), 618–634. https://doi.org/10.1017/S0016756815000758

23. Vosoughi Moradi, A., Sarı, A., Akkaya, P. Geochemistry of the Miocene oil shale (Hançili Formation) in the Çankırı-Çorum Basin, Central Turkey: implications for paleoclimate conditions, source–area weathering, provenance and tectonic setting. *Sedimentary Geology*, 2016, **341**, 289–303. https://doi.org/10.1016/j.sedgeo.2016.05.002
24. Li, Q., Wu, S., Xia, D., You, X., Zhang, H., Lu, H. Major and trace element geochemistry of the lacustrine organic-rich shales from the Upper Triassic Chang 7 Member in the southwestern Ordos Basin, China: implications for paleoenvironment and organic matter accumulation. *Marine and Petroleum Geology*, 2020, **111**, 852–867. https://doi.org/10.1016/j.marpetgeo.2019.09.003
25. Boynton, W. V. Cosmochemistry of the rare earth elements: meteorite studies. In *Rare Earth Element Geochemistry* (Henderson, P., ed.). Elsevier, Amsterdam, 1984, 63–114.
26. Taylor, S. R., McLennan, S. M. *The Continental Crust: Its Composition and Evolution*. Blackwell Scientific Publications, Oxford, 1985.
27. McLennan, S. M. Relationships between the trace element composition of sedimentary rocks and upper continental crust. *Geochemistry, Geophysics, Geosystems*, 2001, **2**(4), 2000GC00010. https://doi.org/10.1029/2000GC000109
28. Han, S., Zhang, Y., Huang, J., Rui, Y., Tang, Z. Elemental geochemical characterization of sedimentary conditions and organic matter enrichment for Lower Cambrian shale formations in northern Guizhou, South China. *Minerals*, 2020, **10**(9), 793. https://doi.org/10.3390/min10090793
29. Godoy, L. H., de Souza Sardinha, D. S., Torres Moreno, M. M. Major and trace elements redistribution in weathered claystones from the Corumbataí Formation, Paraná Sedimentary Basin, São Paulo, Brazil. *Brazilian Journal of Geology*, 2017, **47**(4), 615–632. https://doi.org/10.1590/2317-4889201720170086
30. Kašanin-Grubin, M. *Sedimentology of the Oil Shales Series of the Aleksinac Basin.* M.S. thesis. University of Belgrade, Serbia, 1996.
31. Obradović, J., Vasić, N. *Jezerski baseni u neogenu Srbije*. Srpska akademija nauka i umetnosti, Beograd, 2007.
32. Hay, R. L., Sheppard, R. A. Occurrence of zeolites in sedimentary rocks: an overview. *Reviews in Mineralogy and Geochemistry*, 2001, **45**(1), 217–234. https://doi.org/10.2138/rmg.2001.45.6
33. Wang, Q., Bai, J., Ge, J., Wei, Y., Li, S. Geochemistry of rare earth and other trace elements in Chinese oil shale. *Oil Shale*, 2014, **31**(3), 266–277. https://doi.org/10.3176/oil.2014.3.06
34. Bai, Y., Lv, Q., Liu, Z., Sun, P., Xu, Y., Meng, J. et al. Major, trace and rare earth element geochemistry of coal and oil shale in the Yuqia area, Middle Jurassic Shimengou Formation, northern Qaidam Basin. *Oil Shale*, 2020, **37**(1), 1–31. https://doi.org/10.3176/oil.2020.1.01
35. Cullers, R. L., Graf, J. L. Rare earth elements in igneous rocks of the continental crust: intermediate and silicic rocks – ore petrogenesis. In *Rare Earth Element Geochemistry* (Henderson, P., ed.). Elsevier, Amsterdam, 1984, 275–312.
36. Xu, J.-B., Cheng, B., Deng, Q., Liang, Y.-G., Faboya, O. L., Liao, Z.-W.

Distribution and geochemical significance of trace elements in shale rocks and their residual kerogens. *Acta Geochimica*, 2018, **37**, 886–900. https://doi.org/10.1007/s11631-018-0297-0

37. Bai, Y., Liu, Z., Sun, P., Liu, R., Hu, X., Zhao, H. et al. Rare earth and major element geochemistry of Eocene fine-grained sediments in oil shale- and coal-bearing layers of the Meihe Basin, Northeast China. *Journal* of *Asian Earth Sciences*, 2015, **97**, 89–101. https://doi.org/10.1016/j.jseaes.2014.10.008
38. Bhatia, M. R. Composition and classification of Paleozoic flysch mudrocks of eastern Australia: implications in provenance and tectonic setting interpretation. *Sedimentary Geology*, 1985, **41**(2–4), 249–268. https://doi.org/10.1016/0037-0738(84)90065-4
39. Bhatia, M. R., Crook, K. A. W. Trace element characteristics of graywackes and tectonic setting discrimination of sedimentary basins. *Contributions to Mineralogy and Petrology*, 1986, **92**, 181–193. https://doi.org/10.1007/BF00375292
40. Roser, B. P., Korsch, R. J. Determination of tectonic setting of sandstone-mudstone suites using SiO_2 content and K_2O/Na_2O ratio. *The Journal of Geology*, 1986, **94**(5), 635–650. https://doi.org/10.1086/629071
41. Liu, B., Song, Y., Zhu, K., Su, P., Ye, X., Zhao, W. Mineralogy and element geochemistry of salinized lacustrine organic-rich shale in the Middle Permian Santanghu Basin: implications for paleoenvironment, provenance, tectonic setting and shale oil potential. *Marine and Petroleum Geology*, 2020, **120**, 104569. https://doi.org/10.1016/j.marpetgeo.2020.104569
42. Grizelj, A., Peh, Z., Tibljaš, D., Kovačić, M., Kurečić, T. Mineralogical and geochemical characteristics of Miocene pelitic sedimentary rocks from the south-western part of the Pannonian Basin System (Croatia): implications for provenance studies. *Geoscience Frontiers*, 2017, **8**(1), 65–80. https://doi.org/10.1016/j.gsf.2015.11.009
43. Marović, M., Djoković, I., Pešić, L., Radovanović, S., Toljić, M., Gerzina, N. Neotectonics and seismicity of the southern margin of the Pannonian basin in Serbia. *EGU Stephan Mueller Special Publication Series*, 2002, **3**, 277–295. https://smsps.copernicus.org/articles/3/277/2002/
44. Dimitrijević, M. D. *Geologija Jugoslavije (Geology of Yugoslavia)*. Geological Institute–GEMINI, Belgrade, 1997.
45. Zhang, W. Z., Yang, H., Li, J. F., Ma, J. Leading effect of high-class source rock of Chang 7 in Ordos Basin on enrichment of low permeability oil-gas accumulation – hydrocarbon generation and expulsion mechanism. *Petroleum Exploration and Development*, 2006, **33**(3), 289–293.
46. Westall, F., Campbell, K. A., Bréhéret, J. G., Foucher, F., Gautret, P., Hubert, A. et al. Archean (3.33 Ga) microbe-sediment systems were diverse and flourished in a hydrothermal context. *Geology*, 2015, **43**(7), 615–618. https://doi.org/10.1130/G36646.1
47. Cronan, D. S. *Underwater Minerals*. Academic Press, London, 1980.
48. Pelleter, E., Fouquet, Y., Etoubleau, J., Cheron, S., Labanieh, S., Josso, P. et al.

Ni-Cu-Co-rich hydrothermal manganese mineralization in the Wallis and Futuna back-arc environment (SW Pacific). *Ore Geology Reviews*, 2017, **87**, 126–146. https://doi.org/10.1016/j.oregeorev.2016.09.014

49. Liu, H., Wang, C., Li, Y., Deng, J., Deng, B., Feng, Y. et al. Geochemistry of the black rock series of lower Cambrian Qiongzhusi Formation, SW Yangtze Block, China: reconstruction of sedimentary and tectonic environments. *Open Geosciences*, 2021, **13**(1), 166–187. https://doi.org/10.1515/geo-2020-0228
50. Toth, J. R. Deposition of submarine crusts rich in manganese and iron. *GSA Bulletin*, 1980, **91**(1), 44–54. https://doi.org/10.1130/0016-7606(1980)91<44:DOSCRI>2.0.CO;2
51. Wang, Z., Li, W., Wang, J., Wei, H., Fu, X., Song, C. et al. Controls on organic matter accumulation in marine mudstones from the Lower Permian Zhanjin Formation of the Qiangtang Basin (Tibet), eastern Tethys. *Marine and Petroleum Geology*, 2022, **138**, 105556. https://doi.org/10.1016/j.marpetgeo.2022.105556
52. Alderton, D. Zeolites. In *Encyclopedia of Geology*, *2nd ed.* (Alderton, D., Elias, S. A., eds). Academic Press, London, 2021, 313–325. https://doi.org/10.1016/B978-0-08-102908-4.00041-2
53. Dekov, V. M., Darakchieva, V. Y., Billström, K., Garbe-Schönberg, C. D., Kamenov, G. D., Gallinari, M. et al. Element enrichment and provenance of the detrital component in Holocene sediments from the western Black Sea. *Oceanologia*, 2020, **62**(2), 139–163. https://doi.org/10.1016/j.oceano.2019.10.001
54. Dymond, J., Suess, E., Lyle, M. Barium in deep-sea sediment: a geochemical proxy for paleoproductivity. *Paleoceanography and Paleoclimatology*, 1992, **7**(2), 163–181. https://doi.org/10.1029/92PA00181
55. Ferriday, T., Montenari, M. Chemostratigraphy and chemofacies of source rock analogues: a high-resolution analysis of black shale successions from the lower Silurian Formigoso Formation (Cantabrian Mountains, NW Spain). In *Stratigraphy & Timescales* (Montenari, M., ed.). Elsevier Science, Amsterdam, 2016, 123–255.
56. Tribovillard, N., Algeo, T. J., Lyons, T. W., Riboulleau, A. Trace metals as paleoredox and paleoproductivity proxies: an update. *Chemical Geology*, 2006, **232**(1–2), 12–32. https://doi.org/10.1016/j.chemgeo.2006.02.012
57. Goldberg, K., Humayun, M. 2016. Geochemical palaeoredox indicators in organic-rich shales of the Irati Formation, Permian of the Paraná Basin, southern Brazil. *Brazilian Journal of Geology*, 2016, **46**(3), 377–393. https://doi.org/10.1590/2317-4889201620160001
58. Algeo, T. J., Maynard, J. B. Trace-element behaviour and redox facies in core shales of Upper Pennsylvanian Kansas-type cyclothems. *Chemical Geology*, 2004, **206**(3–4), 289–318. https://doi.org/10.1016/j.chemgeo.2003.12.009
59. Murphy, A. E., Sageman, B. B., Hollander, D. J., Lyons, T. W., Brett, C. E. Black shale deposition and faunal overturn in the Devonian Appalachian Basin: clastic starvation, seasonal water-column mixing, and efficient biolimiting nutrient recycling. *Paleoceanography and Paleoclimatology*, 2000, **15**(3), 280–291. https://doi.org/10.1029/1999PA000445

60. Zhao, J., Jin, Z., Jin, Z., Geng, Y., Wen, X., Yan, C. Applying sedimentary geochemical proxies for paleoenvironment interpretation of organic-rich shale deposition in the Sichuan Basin, China. *International Journal of Coal Geology*, 2016, **163**, 52–71. https://doi.org/10.1016/j.coal.2016.06.015
61. Yamamoto, K. Geochemical characteristics and depositional environments of cherts and associated rocks in the Franciscan and Shimanto Terranes. *Sedimentary Geology*, 1987, **52**(1–2), 65–108. https://doi.org/10.1016/0037-0738(87)90017-0
62. Rimmer, S. M. Geochemical paleoredox indicators in Devonian–Mississippian black shales, Central Appalachian Basin (USA). *Chemical Geology*, 2004, **206**(3–4), 373–391. https://doi.org/10.1016/j.chemgeo.2003.12.029
63. Brumsack, H.-J. The trace metal content of recent organic carbon-rich sediments: implications for Cretaceous black shale formation. *Palaeogeography, Palaeoclimatology, Palaeoecology*, 2006, **232**(2–4), 344–361. https://doi.org/10.1016/j.palaeo.2005.05.011
64. Nagarajan, R., Madhavaraju, J., Nagendra, R., Armstrong-Altrin, J. S., Moutte, J. Geochemistry of Neoproterozoic shales of the Rabanpalli Formation, Bhima Basin, Northern Karnataka, southern India: implications for provenance and paleoredox conditions. *Revista Mexicana de Ciencias Geológicas*, 2007, **24**(2), 150–160.
65. Ross, D. J. K., Bustin, R. M. Investigating the use of sedimentary geochemical proxies for paleoenvironment interpretation of thermally mature organic-rich strata: examples from the Devonian–Mississippian shales, Western Canadian Sedimentary Basin. *Chemical Geology*, 2009, **260**(1–2), 1–19. https://doi.org/10.1016/j.chemgeo.2008.10.027
66. Sajid, Z., Ismail, M. S., Zakariah, M. N. A., Tsegab, H., Gámez Vintaned, J. A., Hanif, T. et al. Impact of paleosalinity, paleoredox, paleoproductivity/preservation on the organic matter enrichment in black shales from Triassic turbidites of Semanggol Basin, Peninsular Malaysia. *Minerals*, 2020, **10**(10), 915. https://doi.org/10.3390/min10100915
67. Kidder, D. L., Erwin, D. H. Secular distribution of biogenic silica through the Phanerozoic: comparison of silica-replaced fossils and bedded cherts at the series level. *The Journal of Geology*, 2001, **109**(4), 509–522. https://doi.org/10.1086/320794
68. Magnall, J. M., Gleeson, S. A., Paradis, S. The importance of siliceous radiolarian-bearing mudstones in the formation of sediment-hosted Zn-Pb ± Ba mineralization in the Selwyn Basin, Yukon, Canada. *Economic Geology*, 2015, **110**(8), 2139–2146. https://doi.org/10.2113/econgeo.110.8.2139
69. Liang, Y., Zhang, J., Liu, Y., Tang, X., Li, Z., Ding, J. et al. Evidence for biogenic silica occurrence in the Lower Silurian Longmaxi Shale in southeastern Chongqing, China. *Minerals*, 2020, **10**(11), 945. https://doi.org/10.3390/min10110945
70. Qin, J., Tao, G., Teng, G. Hydrocarbon-forming organisms in excellent marine source rocks in South China. *Petroleum Geology & Experiment*, 2010, **32**(3), 262–269. https://doi.org/10.11781/sysydz201003262

71. Wu, C., Tuo, J., Zhang, M., Liu, Y., Xing, L., Gong, J., Qiu, J. Multiple controlling factors of lower Palaeozoic organic-rich marine shales in the Sichuan Basin, China: evidence from minerals and trace elements. *Energy Exploration & Exploitation*, 2017, **35**(5), 627–644. https://doi.org/10.1177/0144598717709667
72. Zhang, M., Liu, Z., Xu, S., Sun, P., Hu, X. Element response to the ancient lake information and its evolution history of argillaceous source rocks in the Lucaogou Formation in Sangonghe area of southern margin of Junggar Basin. *Journal of Earth Science*, 2013, **24**, 987–996. https://doi.org/10.1007/s12583-013-0392-4
73. Ma, L., Zhang, Z., Meng, W. Climate-provenance effect on the organic matter enrichment of the Chang 9 source rocks in the Central Ordos Basin, China. *Geofluids*, 2021, **2021**(1), 1233879. https://doi.org/10.1155/2021/1233879
74. Zhao, Z. Y., Zhao, J. H., Wang, H. J., Liao, J. D., Liu, C. M. Distribution characteristics and applications of trace elements in Junggar Basin. *Natural Gas Exploration and Development*, 2007, **30**, 30–33.
75. Wang, J.-X., Sun, P.-C., Liu, Z.-J., Li, Y.-J. Characteristics and genesis of lacustrine laminar coal and oil shale: a case study in the Dachanggou Basin, Xinjiang, Northwest China. *Marine and Petroleum Geology*, 2021, **126**, 104924. https://doi.org/10.1016/j.marpetgeo.2021.104924
76. Jin, Z. D., Zhang, E. L. Paleoclimate implications of Rb/Sr ratios from lake sediments. *Science and Technology Engineering*, 2002, **2**(3), 20–22.
77. Zuo, X., Li, C., Zhang, J., Ma, G., Chen, P. Geochemical characteristics and depositional environment of the Shahejie Formation in the Binnan Oilfield, China. *Journal of Geophysics and Engineering*, 2020, **17**(3), 539–551. https://doi.org/10.1093/jge/gxaa013
78. Lerman, A. *Lakes: Chemistry, Geology, Physics*. Springer, New York, 1978.
79. Armstrong-Altrin, J., Lee, Y. I., Kasper-Zubillaga, J. J., Trejo-Ramírez, E. Mineralogy and geochemistry of sands along the Manzanillo and El Carrizal beach areas, southern Mexico: implications for palaeoweathering, provenance and tectonic setting. *Geological Journal*, 2017, **52**(4), 559–582. https://doi.org/10.1002/gj.2792
80. Tenger, B., Liu, W., Xu, Y., Gao, C., Hu, K., Gao, C. Comprehensive geochemical identification of highly evolved marine hydrocarbon source rocks: organic matter, paleoenvironment and development of effective hydrocarbon source rocks. *Chinese Journal of Geochemistry*, 2006, **25**, 333–340. https://doi.org/10.1007/s11631-006-0332-4
81. Wei, Y., Li, X., Zhang, R., Li, X., Lu, S., Qiu, Y. et al. Influence of a paleosedimentary environment on shale oil enrichment: a case study on the Shahejie Formation of Raoyang Sag, Bohai Bay Basin, China. *Frontiers of Earth Science*, 2021, **9**, 736054. https://doi.org/10.3389/feart.2021.736054
82. Liu, Y. J., Cao, L. M., Li, Z. L., Wang, H. N., Chu, T. Q., Zhang, J. R. *Element Geochemistry*. Science Press, Beijing, 1984.
83. Torres, M. E., Brumsack, H. J., Bohrmann, G., Emeis, K. C. Barite fronts in continental margin sediments: a new look at barium remobilization in the

zone of sulfate reduction and formation of heavy barites in diagenetic fronts. *Chemical Geology*, 1996, **127**(1–3), 125–139. https://doi.org/10.1016/0009-2541(95)00090-9

84. Reimann, C., Caritat, P. *Chemical Elements in the Environment*. Springer, Berlin, 1998.
85. Xu, B., Ding, S., Wang, Y., Liu, Q. F. Geochemical characteristics of illite clay rocks from the Shihezi Formation in the Hanxing mining area and its sedimentary environment. *Mining Science and Technology (China)*, 2011, **21**(4), 495–500. https://doi.org/10.1016/j.mstc.2011.06.006
86. Deng, H. W., Qian, K. *Sedimentary Geochemistry and Environment Analysis*. Gansu Technology Publishing House, Lanzhou, 1993.
87. Sun, Z. C., Yang, P., Zhang, Z. H. *Sedimentary Environment and Hydrocarbon Generation of China Cenozoic Salty Lacustrine Facies*. Petroleum Industry Press, Beijing, 1997.
88. Lan, X. H., Ma, D. X., Xu, M. G., Zhou, Q. W., Zhang, G. W. Some geochemical signs and their importance for sedimentary facies. *Marine Geology & Quaternary Geology*, 1987, **7**(1), 39–49.
89. Zheng, R. C., Liu, M. Q. Study on paleosalinity of Chang-6 oil reservoir set in Ordos Basin. *Oil and Gas Geology*, 1999, **20**(1), 20–25.
90. Meng, Q. T., Liu, Z. J., Bruch, A. A., Liu, R., Hu, F. Palaeoclimatic evolution during Eocene and its influence on oil shale mineralisation, Fushun basin, China. *Journal* of *Asian Earth Sciences,* 2012, **45**, 95–105. https://doi.org/10.1016/j.jseaes.2011.09.021
91. Hunt, J. M. *Petroleum Geochemistry and Geology*. W. H. Freeman and Company, San Francisco, 1979.
92. Holland, H. D. *The Chemistry of the Atmosphere and the Oceans*. Wiley-Interscience, New York, 1978.
93. Morford, J. L., Russell, A. D., Emerson, S. Trace metal evidence for changes in the redox environment associated with the transition from terrigenous clay to diatomaceous sediment, Saanlich Inlet, BC. *Marine Geology*, 2001, **174**(1–4), 355–369. https://doi.org/10.1016/S0025-3227(00)00160-2
94. Li, Y., Wang, Z., Gan, Q., Niu, X., Xu, W. Paleoenvironmental conditions and organic matter accumulation in Upper Palaeozoic organic-rich rocks in the east margin of the Ordos Basin, China. *Fuel*, 2019, **252**, 172–187. https://doi.org/10.1016/j.fuel.2019.04.095
95. Hetzel, A., März, C., Vogt, C., Brumsack, H.-J. Geochemical environment of Cenomanian–Turonian black shale deposition at Wunstorf (northern Germany). *Cretaceous Research*, 2011, **32**(4), 480–494. https://doi.org/10.1016/j.cretres.2011.03.004
96. Jones, B., Manning, D. A. C. Comparison of geochemical indices used for the interpretation of palaeoredox conditions in ancient mudstones. *Chemical Geology*, 1994, **111**(1–4), 111–129. https://doi.org/10.1016/0009-2541(94)90085-X
97. Wang, Z., Fu, X., Feng, X., Song, C., Wang, D., Chen, W. et al. Geochemical features of the black shales from the Wuyu Basin, southern Tibet: implications

for palaeoenvironment and palaeoclimate. *Geological Journal*, 2017, **52**(2), 282–297. https://doi.org/10.1002/gj.2756

98. Sun, Y.-Z., Jinxi, W., Shifeng, L., Kankun, J., Mingyue, L. Mechanism of uranium accumulation in the Kupferschiefer from Poland and Germany. *Energy Exploration & Exploitation*, 2005, **23**(6), 463–473. https://doi.org/10.1260/014459805776986902
99. Chen, R., Sharma, S., Bank, T., Soeder, D., Eastman, H. Comparison of isotopic and geochemical characteristics of sediments from a gas- and liquids-prone wells in Marcellus Shale from Appalachian Basin, West Virginia. *Applied Geochemistry*, 2015, **60**, 59–71. https://doi.org/10.1016/j.apgeochem.2015.01.001
100. Khan, M. Z., Feng, Q., Zhang, K., Guo, W. Biogenic silica and organic carbon fluxes provide evidence of enhanced marine productivity in the Upper Ordovician-Lower Silurian of South China. *Palaeogeography, Palaeoclimatology, Palaeoecology*, 2019, **534**, 109278. https://doi.org/10.1016/j.palaeo.2019.109278
101. Li, Y., Wang, N., Li, Z., Zhou, X., Zhang, C., Wang, Y. Carbonate formation and water level changes in a paleo-lake and its implication for carbon cycle and climate change, arid China. *Frontiers of Earth Science*, 2013, **7**, 487–500. https://doi.org/10.1007/s11707-013-0392-9
102. Glikson, M., Chappell, B. W., Freeman, R. S., Webber, E. Trace elements in oil shales, their source and organic association with particular reference to Australian deposits. *Chemical Geology*, 1985, **53**(1–2), 155–174. https://doi.org/10.1016/0009-2541(85)90028-2
103. Fu, X., Wang, J., Zeng, Y., Tan, F., Feng, X. Concentration and mode of occurrence of trace elements in marine oil shale from the Bilong Co area, northern Tibet, China. *International Journal of Coal Geology*, 2011, **85**(1), 112–122. https://doi.org/10.1016/j.coal.2010.10.004
104. Chowdhury, A. N., Handa, B. K., Das, A. K. High lithium, rubidium and cesium contents of thermal spring water, spring sediments and borax deposits in Puga valley, Kashmir, India. *Geochemical Journal*, 1974, **8**(2), 61–65. https://doi.org/10.2343/geochemj.8.61
105. Fleet, A. J., Kelts, K., Talbot, M. R. *Lacustrine Petroleum Source Rocks*. Geological Society of London, Special Publications No. 40, London, 1988.
106. Katz, B. J. Factors controlling the development of lacustrine petroleum source rocks – an update. In *Paleogeography, Paleoclimate, and Source Rocks* (Huc, A.-Y., ed.). American Association of Petroleum Geologists, Studies in Geology 40, 1995, 61–79.
107. Rosen, B. H., Loftin, K. A., Graham, J. L., Stahlhut, K. N., Riley, J. M., Johnston, B. D. et al. *Understanding the Effect of Salinity Tolerance on Cyanobacteria Associated With a Harmful Algal Bloom in Lake Okeechobee, Florida*. U.S. Geological Survey Scientific Investigations Report, 2018, 2018–5092, 32. https://doi.org/10.3133/sir20185092
108. Schwarzbauer, J., Jovančićević, B. *Fossil Matter in the Geosphere*. Springer, Heidelberg, 2015.